Journal of Physics: Conference Series

PAPER • OPEN ACCESS

CFD Analysis of a Finite Linear Array of Savonius Wind Turbines

To cite this article: Belabes Belkacem and Marius Paraschivoiu 2016 *J. Phys.: Conf. Ser.* **753** 102008

CFD Analysis of a Finite Linear Array of Savonius Wind Turbines

Belabes Belkacem [1] and Marius Paraschivoiu [2]

[1] Centre de Développement des Energies Renouvelables, 16340 Algiers, Algeria
[2] Concordia University, Montréal, H3G1M8, Québec, Canada

e-mail: marius.paraschivoiu@concordia.ca (M. Paraschivoiu).

Abstract. Vertical axis wind turbines such as Savonius rotors have been shown to be suitable for low wind speeds normally associated with wind resources in all corners of the world. However, the efficiency of the rotor is low. This paper presents results of Computational Fluid Dynamics (CFD) simulations for an array of Savonius rotors that show a significant increase in efficiency. It looks at identifying the effect on the energy yield of a number of turbines placed in a linear array. Results from this investigation suggest that an increase in the energy yield could be achieved which can reach almost two times than the conventional Savonius wind turbine in the case of an array of 11turbines with a distance of 1.4R in between them. The effect of different TSR values and different wind inlet speeds on the farm has been studied for both a synchronous and asynchronous wind farm.

Key Words: Savonius Rotor; Multiple Turbines; Power Coefficient; Computational Fluid Dynamic (CFD)

1. Introduction

The Savonius rotor is simple in structure, has good starting characteristics, relatively low operating speeds, and an ability to accept wind from any direction. Its aerodynamic efficiency is lower than that of other types of wind turbines, such as Darrieus and propeller rotors. The concept of the Savonius rotor is based on the principle developed by Flettner/Savonius [1] who claimed maximum coefficient of power 0.37 based on field trials. However, this performance has not been achieved by subsequent researchers. This turbine uses the drag force acting on its blades, however, at low angle of attacks, lift force also contributes to torque production [2]. Recently, some numerical studies are aimed at improving the performance of VAWT using Computational Fluid Dynamics (CFD) technique. El-Baz et al. [3] proposed a Savonius rotor which has higher power coefficient compared with the conventional rotor. The peak power coefficient of the novel design of Savonius rotor turbine is 44% higher than that of the original rotor. Another designs proposed by El-Askary et al. [4] suggested performance to reach a power-coefficient peak of 0.52. Also, Goh et al.[5] installed a turbine above a bluff body to improve its power coefficient (Cp). The Cp calculated using these derived free stream wind speeds showed an increase of 25% at 12 m/s wind speed, compared to the Cp reported by previous researchers for a similar turbine operating in unmodified air flow. The Savonius turbine however suffers from poor efficiency. The power coefficient of conventional Savonius turbines is around 0.21 which is low compared to other vertical turbines. In recent literature [6], the interaction between adjacent turbines has shown to effectively increase the extracted power. This concept is further explored and a study is proposed to find configurations of Savonius turbines to achieve higher performance. The study analysis the results of 3D simulations based on CFD for 5 and 11 turbines in a linear array. Also, this work describes the validation of the simulation with experimental data from Hayashi (2005) [7] for different incoming flow velocities.

2. Savonius Turbine

The Savonius rotor consists of two semi buckets that are placed in opposite opened section separated by a gap and an overlap ratio as shown in Figure 1, where H, R and d are the height, radius and diameter respectively of the Savonius turbine rotor geometry used in this study. The values of these parameters are shown in table 1, but the distance gap between turbines, D, changes in each case study.

Table 1. Geometry sizes

H	2.43 m
D	0.33 m
R	0.165 m
X1	-1.233R
Y1	-0.454R
X2	-1.099R
Y2	-1.1770R

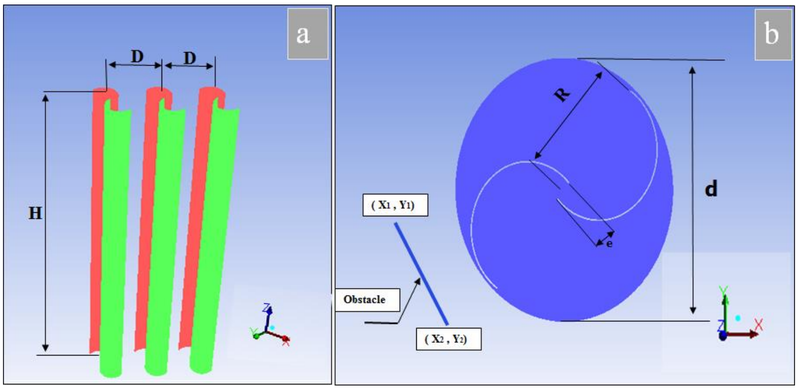

Figure 1. Schematic of a Savonius rotor. **(a)** Front view; **(b)** top view.

3. Performance of Savonius turbines

The Savonius rotor is very robust, simple to construct and is characterized by a high starting torque [8, 9]. It has many advantages, including a simple design, and the ability to operate in any wind direction, though it has a low aerodynamic efficiency [10, 11]. Table 1 and figure 1 detail the geometry of the semi-circular Savonius rotor and the obstacle used in the present study.
The aspect ratio β of the Savonius rotor is defined as:

$$\beta = \frac{H}{R} \tag{1}$$

where H and R are the rotor height and the semi-bucket diameter respectively. Ushiyama, Nagai and Shinoda (1986) reported an optimum value of 4.29 [12]. Further studies by other researchers (Hayashi et al. [6] and Kamoji et al. [13]) used lower ratios such as 1.2 due to wind tunnel blockage effect.
Another important parameter is the overlap ratio, which is defined in equations (2):

$$\varepsilon = \frac{e}{R} \tag{2}$$

where 'ε' is the overlap ratio and e is the overlap length as shown in figure 1. The power coefficient of a Savonius turbine is higher for an overlap ratio between 0.1 to 0.15 as reported by Blackwell, Sheldahl and Feltz, [14] while it decreases when the overlap ratio is less than 0.1 and larger than 0.3. Between the range 0.15 to 0.3, another study done by Menet (2004) [15, 16] found that the optimum performance was for an overlap ratio in the range of 0.2 to 0.25. Yaakob, Tawi and Suprayogi [17] found similar results. The highest torque in their studies was reported in an overlap ratio of 0.21. Thus the overlap of the Savonius rotor in this study is chosen to be 0.206 in all cases.
The use of end plate increases the rotor performance as recommended by Ogawa and Yoshida [18]. It was also noted by Menet [15, 16] that an end plate which is 10% larger than the rotor diameter, D, leads to a higher value of the power coefficient. The tip speed ratio λ or TSR is defined as the ratio between the rotational speed of the tip of the blade and the actual velocity of the wind such as in equation (3) [19-23]:

$$\lambda = \frac{\omega d}{2U} \tag{3}$$

The air at velocity U produces mechanical torque T and mechanical power P on a turbine. By defining the swept area (As) for the Savonius rotor as the height H multiplied by diameter d, the torque coefficient is given in equations (4) [22-25]:

$$Cm = \frac{T}{\frac{1}{4}\rho A_s d U^2} \tag{4}$$

and the power coefficient is given in equation (5) [20, 22-27]:

$$Cp = \frac{P}{\frac{1}{2}\rho A_s U^3} \tag{5}$$

The efficiency of the turbine will be measured using these parameters as a function of TSR. Typical Savonius turbines have a low power coefficient with a typical maximum values around 0.2. Current successful commercial turbines have a power coefficient higher than 0.35 and as high as 0.5 for large Horizontal Axis Wind Turbines. The analysis of the conventional Savonius rotor with respect to different gap distances (D), placed in an array, will be performed to increase the power coefficient.

4. CFD simulations

The flow simulations presented in this work are based on the ANSYS Fluent 15.0 code. For these 3D simulations, the unsteady Reynolds-Averaged Navier-Stokes equations are solved using the SIMPLE (Semi-Implicit Method for Pressure-Linked Equations) algorithm for pressure-velocity coupling). The second-order upwind scheme is used in the simulation. The unsteady flow is solved by using the Sliding Mesh Model (SMM). Three or more complete revolutions are always computed. Minimum size of the domain uses 20 times the rotor radius on each side of the turbine, i.e. 20R. The outflow boundary was extended at least another half domain size to reduce the backflow effect. It was found that the best turbulence model was the realizable (k-ε) model which shows an excellent agreement between CFD and experimental results for calculating (Cp) [28].

5. Results and Discussion

Validating the simulation results with available experimental was performed by comparison the CFD results with published experimental data given by Hayashi et al. (2005) [6]. A mesh of 1.4 million cells was constructed following a mesh convergence study based on the convergence of the moment coefficient. The comparison presented in Figure 2 indicates slightly overestimate CFD results. It may be noted that there is not a significant change in the results for different wind velocities.

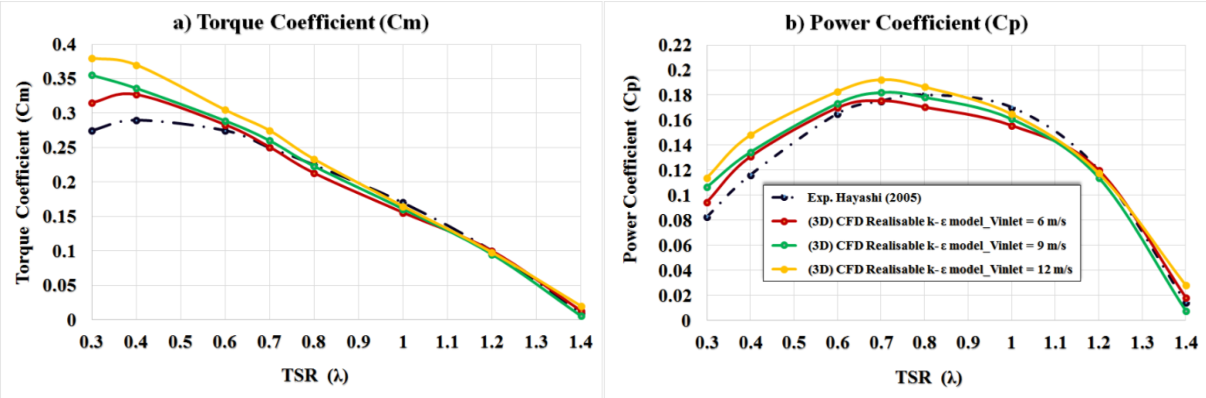

Figure 2. Validation of computational model for conventional Savonius rotor: (a) torque coefficient; (b) power coefficient.

5.1 Effect of rotor number

The array of Savonius turbines is now investigated for three cases: one single turbine, 5 turbines and 11 turbines facing the wind. The configuration is achieved by fixing the distance between their axes at 1.4R. A mesh of 2.48 million cells was used for the case with 5 turbines and a mesh with 5.08 million cells was used for the case with 11 turbines. All the turbines have the same rotation direction and each turbine has a shield on the left side. A very important improvement in this new arrangement is observed for the two array cases investigated. This improved performance is attributed to the favorable interaction between the rotors and the shields that redirect the flow to the adjacent rotors. The power coefficients results for the best turbine in each configuration are plotted in figure 3. To understand the flow pattern, Figure 4 illustrates the pressure contour obtained from the simulation. This figure indicates that the end turbine (top turbine) is not as efficient. To make sure that this increase in not due to a blockage effect from the boundary condition on the sides, three domains with sides at a distance of 66R, 132R and 264R were performed. The difference in the Cp for the entire turbine array at TSR 0.8 is very small: 0.303, 0.306 and 0.290, respectively.

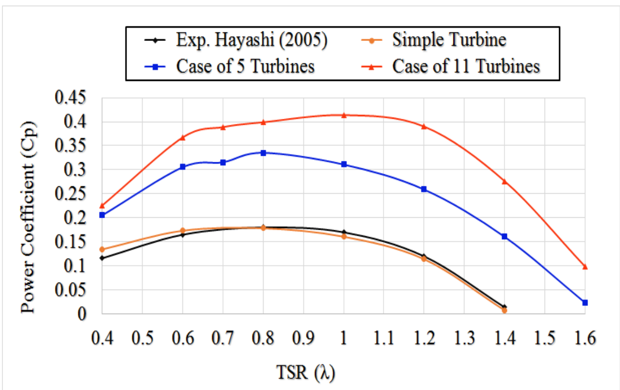

Figure 3. Power coefficient versus tip speed ratio compared between best turbine in each configuration

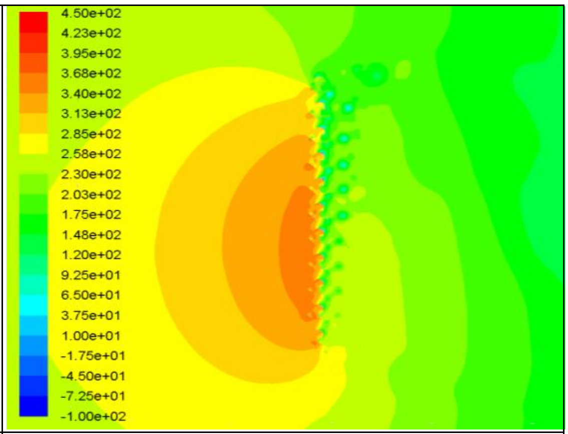

Figure 4. Pressure contour for the case with 11 turbines at TSR =0.8

From figure 3, it can be noticed that the case with 11 turbines has the best power coefficient which is more than double the original turbine.

5.2. Synchronous and Asynchronous Wind power Farm_11T

One can see in figure 4, that the pressure is higher in the middle bottom side of the farm_11T, because this pressure is affected by the obstacles orientation and the synchronous rotation of all the turbines. In this context and to understand this phenomena, two farms with 11 turbines, with the same geometric topology but different slightly different rotation speed between the blades were simulated. In the first farm (named Synchronous), the same rotational velocity for each turbine was used and the same blade position of turbines as shown figure 5, named the Synchronous Farm_11T.
In the second farm a random TSR value between 0.6 and 1.0 was used for each turbine. This farm was named the Asynchronous Farm_11T as the positions of blades of each turbine are completely asynchronous with each other. Both configurations are shown in figure 5. The domain, solver setting and turbulence model are similar between both simulation cases. The same grid topology is used which resulted in a grid having a number of cells equal to 5 083 422 cells for both farms. An important difference in the simulations is the time to convergence: for the Synchronous Farm_11T, the time is 48 hours, while for the second case is more 168 hour on the same computer. This difference is related to the increase unsteadiness as the rotors are not in the same position and no cycle can be defined.

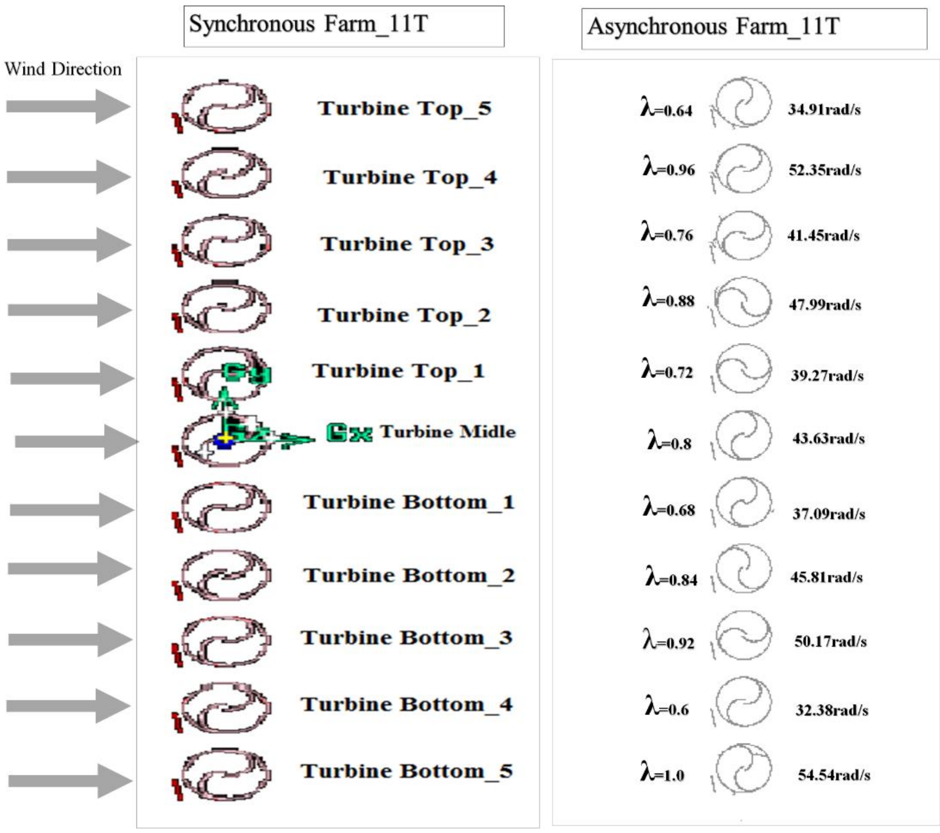

Figure 5. Farm configurations.

5.2.1 *Effect of Tip Speed Ratio (λ)*

Figure 6 presents the pressure and velocity contours for both cases reported for the maximum production of both Farms. One can observe the wake difference between the two cases and the more symmetric flow in the case of the asynchronous farm. This effect helps the end turbines to be more efficient and therefore distributes the energy production to all the turbines.

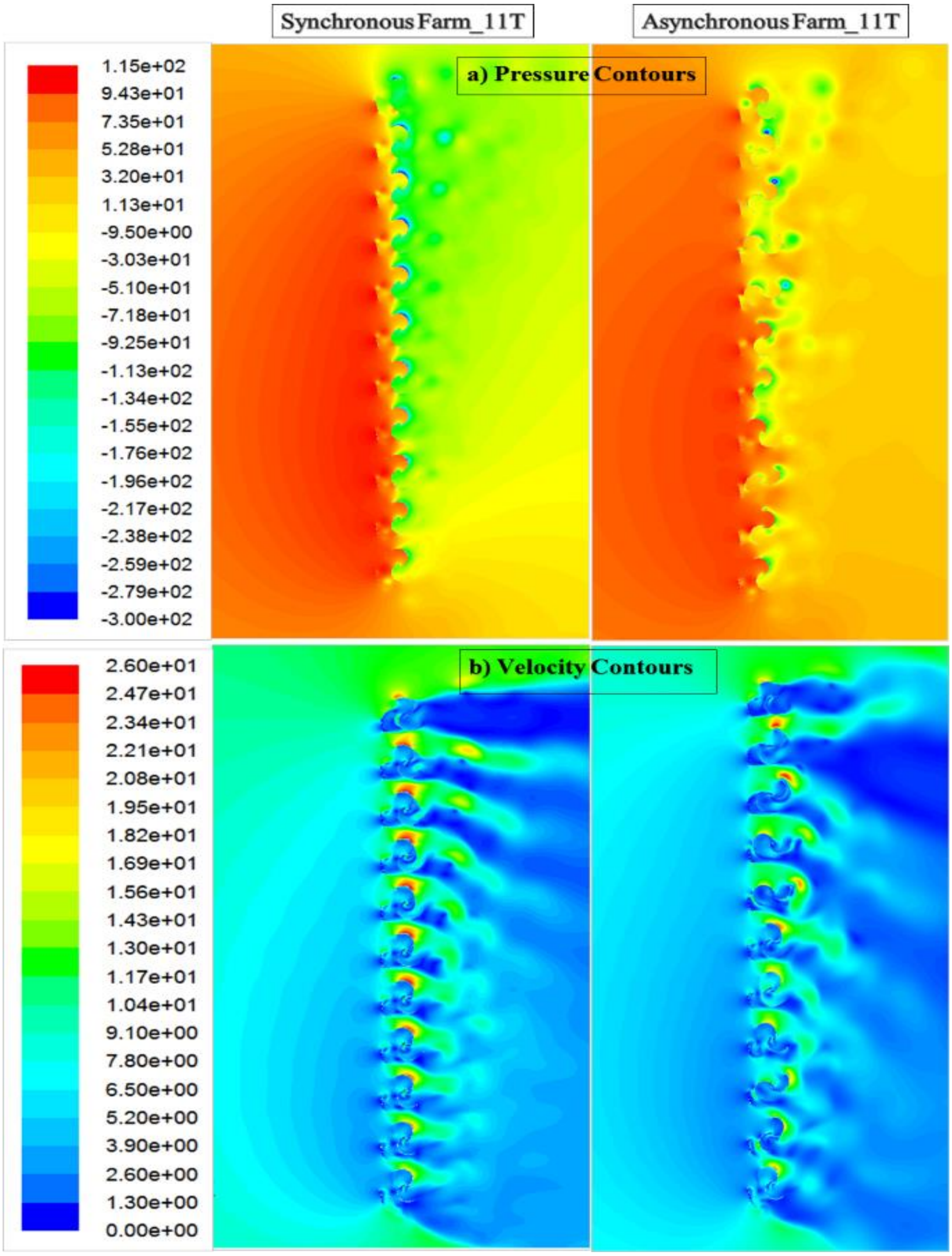

Figure 6. Comparison between Synchronous and Asynchronous Farm_11T contours.

The power coefficient associated with each turbine for both farms is calculated and presented in figure 7. This figure presents the comparison of the power coefficient (Cp) obtained for the asynchronous farms_11T with the inlet velocity of 9 m/s. The (Cp) for three TSR values for the synchronous farm is also reported. The figure clearly shows that there is no significant difference between the (SumCp/11) of both farms, while the maximum power coefficient is concentered in the middle turbines of the synchronous Farm_11T, but the power coefficient is a function of the TSR for the asynchronous Farm_11T. Note that the turbine top 5 and turbine bottom 1 have low Cp because their TSR values are also low, i.e. 0.64 and 0.68 respectively.

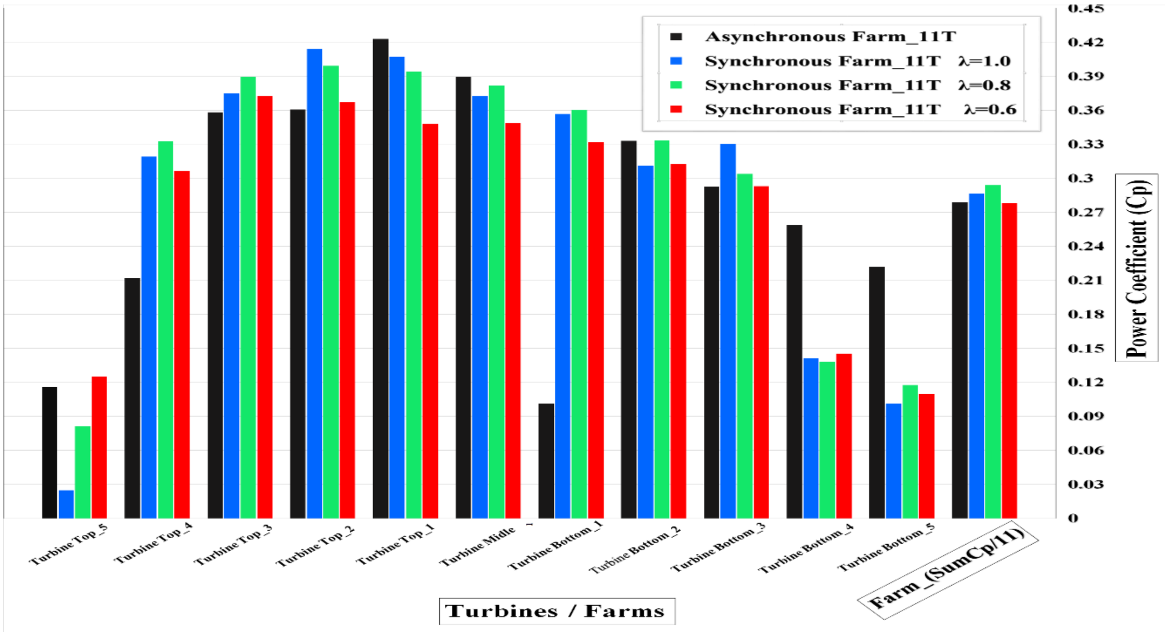

Figure 7. Maximum power coefficient for each wind turbine for the synchronous and asynchronous farm_11T.

The torque variation as the turbines are rotating is shown in Figure 8, for three turbines locations that have the same TSR. These turbines are: Turbine bottom_4, Turbine middle and Turbine bottom_5 which have TSRs: 0.6, 0.8 and 1.0 respectively.

The torque for the last 8 revolutions is compared with the last 2 revolutions for the Synchronous Farm_11T turbine. One can observe the difference between the variation torques for these selected three cases. For all TSRs, the shape of the torque oscillation for the synchronous Farm_11T case is repetitive but for the case of the Asynchronous Farm_11T the shape is not similar as it may be affected differently by the neighboring turbines. These difference result in different values of the Cp as reported in figure 7. The period between peaks is equivalent to the angular rotation for both cases.

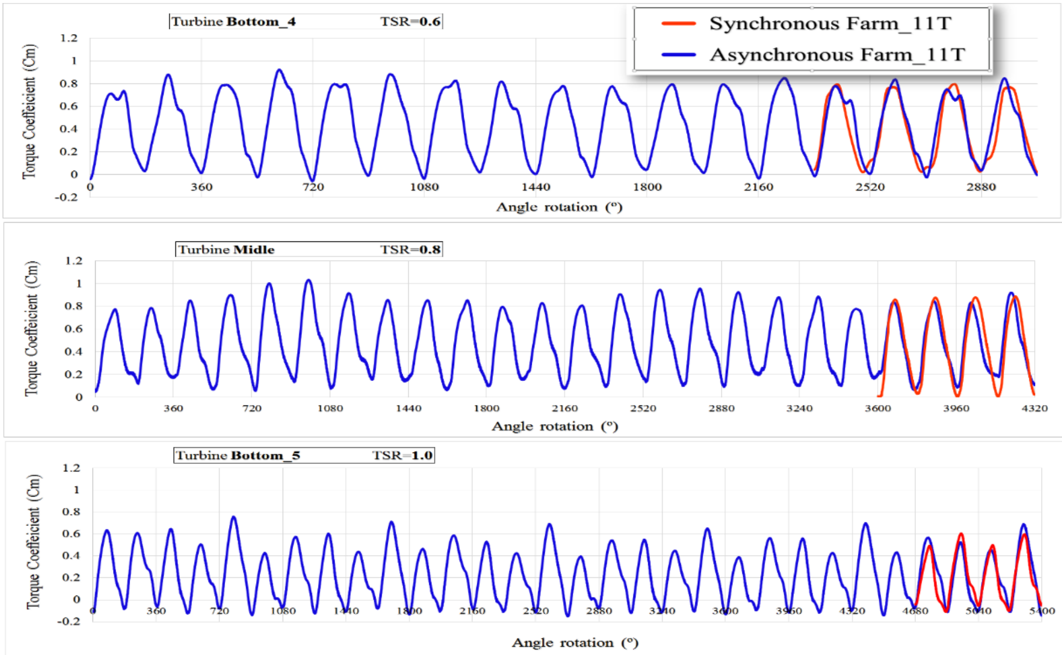

Figure 8. Instantaneous Torque coefficient (Cm) vs Rotational Angle of the Asynchronous Farm_11T compared with the last two Cycles for synchronous Farm_11T.

5.2.2 Velocity inlet effect

In this section the wind velocity is changed: 6, 9 and 12 m/s while keeping the same rotation speed. The average power coefficient for each wind speed is calculated and presented in figure 9. Figure 9 presents a comparison between, the power coefficient obtained for each case, and compared with results obtained for the synchronous Farm_11T as well as the results obtained with for the single turbine both numerically and experimentally. There is a small difference between the results given by a different velocity inlet but nothing very significant. Furthermore for both farms and for all cases, the average power coefficient of the turbines in the farms is higher than the single turbine.

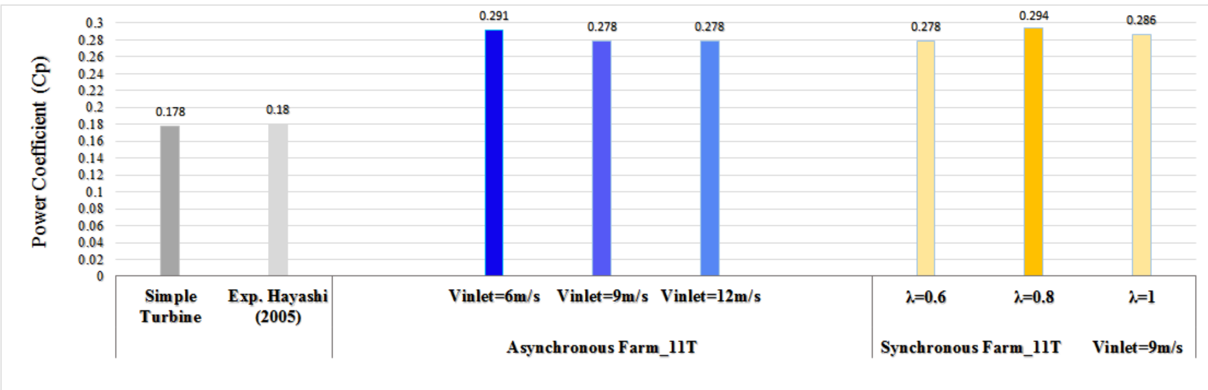

Figure 9. Average Power coefficient for the Asynchronous Farm_11T from different velocity inlet compared with the synchronous Farm_11T, simple turbine and experiment Data.

6. Conclusions

The 3D Computational Fluid Dynamics (CFD) simulations for an array of Savonius rotors has been carried out to investigate the power coefficient extracted from turbines placed in a linear arrangement. The key findings and conclusions based on this work are listed as follows:

- The obtained numerical results using the realizable K-ε model are close to experimental measurements for a single turbine;
- The average power coefficient of each turbine placed in a linear arrangement of Savonius wind turbines is almost 60% higher than those of the conventional Savonius turbine;
- The number of turbines on the farm increase the farm efficient;
- Synchronous and Asynchronous Farms with 11 turbines had no significant difference of the mean power coefficient.
- The Cp calculated for the asynchronous farm_11T is not influenced by the incoming wind velocity;
- The improved performance is attributed to the favorable interaction between the rotors and the shields that redirect the flow to the adjacent rotors.

This work is significant because it demonstrates that an optimized placement of Savonius turbines can lead to high energy production and low land footprint. Additional analysis must be done to investigate the effect of the wind direction.

References

1. Savonius, S.J., *The S-rotor and its applications.* Mech. Eng, 1931. **53**: p. 333-338.
2. Modi, V. and M. Fernando, *On the performance of the Savonius wind turbine.* Journal of solar energy engineering, 1989. **111**(1): p. 71-81.
3. El-Baz, A., K. Youssef, and M. Mohamed, *Innovative improvement of a drag wind turbine performance.* Renewable Energy, 2016. **86**: p. 89-98.
4. El-Askary, W., et al., *Harvesting wind energy for improving performance of Savonius rotor.* Journal of Wind Engineering and Industrial Aerodynamics, 2015. **139**: p. 8-15.
5. Goh, S.C., et al., *Tow testing of Savonius wind turbine above a bluff body complemented by CFD simulation.* Renewable Energy, 2016. **87**: p. 332-345.
6. Sun, X., et al., *Numerical study on coupling effects among multiple Savonius turbines.* Journal of Renewable and Sustainable Energy, 2012. **4**(5): p. 053107.
7. Hayashi, T., Y. Li, and Y. Hara, *Wind tunnel tests on a different phase three-stage Savonius rotor.* JSME International Journal Series B Fluids and Thermal Engineering, 2005. **48**(1): p. 9-16.
8. Kacprzak, K., G. Liskiewicz, and K. Sobczak, *Numerical investigation of conventional and modified Savonius wind turbines.* Renewable energy, 2013. **60**: p. 578-585.
9. Afungchui, D., B. Kamoun, and A. Helali, *Vortical structures in the wake of the savonius wind turbine by the discrete vortex method.* Renewable Energy, 2014. **69**: p. 174-179.
10. Altan, B.D. and M. Atılgan, *The use of a curtain design to increase the performance level of a Savonius wind rotors.* Renewable Energy, 2010. **35**(4): p. 821-829.
11. Jeon, K.S., et al., *Effects of end plates with various shapes and sizes on helical Savonius wind turbines.* Renewable Energy, 2015. **79**: p. 167-176.
12. Ushiyama, I. and H. Nagai, *Optimum design configurations and performance of Savonius rotors.* Wind Engineering, 1988. **12**(1): p. 59-75.
13. Kamoji, M., S. Kedare, and S. Prabhu, *Performance tests on helical Savonius rotors.* Renewable Energy, 2009. **34**(3): p. 521-529.
14. Blackwell, B.F., R.F. Sheldahl, and L.V. Feltz, *Wind tunnel performance data for two-and three-bucket Savonius rotors*. 1977: Sandia Laboratories Springfield, VA, USA.
15. Menet, J.-L. and N. Bourabaa, *Increase in the Savonius rotors efficiency via a parametric investigation.* 2004.
16. Menet, J.-L., *A double-step Savonius rotor for local production of electricity: a design study.* Renewable energy, 2004. **29**(11): p. 1843-1862.

17. Yaakob, O., Y.M. Ahmed, and M.A. Ismail. *Validation study for savonius vertical axis marine current turbine using CFD simulation*. in *Asia-Pacific Workshop on Marine Hydrodynamics, APHydro2012*. 2012.
18. OGAWA, T. and H. YOSHIDA, *The effects of a deflecting plate and rotor end plates on performances of Savonius-type wind turbine.* Bulletin of JSME, 1986. **29**(253): p. 2115-2121.
19. Abraham, J., et al., *Numerical simulation of fluid flow around a vertical-axis turbine.* Journal of Renewable and Sustainable Energy, 2011. **3**(3): p. 033109.
20. Chen, C.-A., T.-Y. Huang, and C.-H. Chen, *Novel plant development of a parallel matrix system of Savonius wind rotors with wind deflector.* Journal of Renewable and Sustainable Energy, 2015. **7**(1): p. 013135.
21. Bai, C.-J., et al., *Computational fluid dynamics analysis of the vertical axis wind turbine blade with tubercle leading edge.* Journal of Renewable and Sustainable Energy, 2015. **7**(3): p. 033124.
22. Debnath, B.K., A. Biswas, and R. Gupta, *Computational fluid dynamics analysis of a combined three-bucket Savonius and three-bladed Darrieus rotor at various overlap conditions.* Journal of Renewable and Sustainable energy, 2009. **1**(3): p. 033110.
23. Sun, X., et al., *A three-dimensional numerical study of the Magnus wind turbine with different blade shapes.* Journal of Renewable and Sustainable Energy, 2012. **4**(6): p. 063139.
24. Gupta, R., A. Biswas, and K. Sharma, *Comparative study of a three-bucket Savonius rotor with a combined three-bucket Savonius–three-bladed Darrieus rotor.* Renewable Energy, 2008. **33**(9): p. 1974-1981.
25. Jaohindy, P., et al., *An analysis of the transient forces acting on Savonius rotors with different aspect ratios.* Renewable Energy, 2013. **55**: p. 286-295.
26. Abraham, J., et al., *Summary of Savonius wind turbine development and future applications for small-scale power generation.* Journal of Renewable and Sustainable Energy, 2012. **4**(4): p. 042703.
27. Zhou, T. and D. Rempfer, *Numerical study of detailed flow field and performance of Savonius wind turbines.* Renewable energy, 2013. **51**: p. 373-381.
28. Mohamed, M., et al., *Optimal blade shape of a modified Savonius turbine using an obstacle shielding the returning blade.* Energy Conversion and Management, 2011. **52**(1): p. 236-242.